Self-diffusion of nonfreezing water in porous carbohydrate polymer systems studied with nuclear magnetic resonance

Topgaard, Daniel; Söderman, Olle

Published in:
Biophysical Journal

2002

Self-Diffusion of Nonfreezing Water in Porous Carbohydrate Polymer Systems Studied with Nuclear Magnetic Resonance

Daniel Topgaard and Olle Söderman
Division of Physical Chemistry 1, Center for Chemistry and Chemical Engineering, Lund University, S-221 00 Lund, Sweden

ABSTRACT Water is an integral part of the structure in biological porous materials such as wood and starch. A problem often encountered in the preparation of samples for, e.g., electron microscopy is that removal of water leads to a decreasing distance between supermolecular structural elements and a distortion of the structure. It is, therefore, of interest to find methods to investigate these materials in the native water-swollen state. We present a method to study water-swollen biological porous structures using NMR to determine the amount and self-diffusion of water within the porous objects. The contribution of bulk water to the NMR signal is eliminated by performing experiments below the bulk freezing temperature. Further decrease of the temperature leads to a gradual freezing of water within the porous objects. The contribution of the freezing water fraction to the migration of water through the porous network is, thus, estimated. The results are rationalized in terms of the ultrastructure of the samples studied, namely, wood pulp fibers and potato starch granules.

INTRODUCTION

Water sorbed in porous materials has thermodynamic properties different from bulk water due to interaction with the porous matrix. Osmotic and capillary effects result in a melting point depression of the sorbed water. The amount of nonfreezing liquid in porous materials as a function of temperature has been investigated with NMR (Overloop and Van Gerven, 1993; Strange et al., 1993; Hansen et al., 1996, 1997; Furó and Daicic, 1999) and differential scanning calorimetry (Ishikiriyama and Todoki, 1995; Maloney and Paulapuro, 1998). The results are usually expressed as pore size distributions where the pore size is related to the melting point depression through the Gibbs-Thomson equation (Jackson and McKenna, 1990). The properties and location of nonfreezing water have been studied by ^{1}H and ^{2}H NMR wideline and relaxation techniques for starch (Tanner et al., 1991; Li et al., 1998; Tang et al., 2000) and cellulose (Vittadini et al., 2001) systems.

In this study, we present a method for the characterization of swelling porous materials in the wet state. In the present context we define a pore as any space large enough to accommodate at least one water molecule. NMR is used to follow the amount and self-diffusion of nonfreezing water as a function of temperature. Different parts of the pore structure is probed through the partial immobility of the pore liquid. NMR diffusometry is a well-established technique for studying the translational motion of liquid state molecules on the micrometer scale. The translational motion of liquids imbibed in a porous medium is affected by the enclosing geometry. Diffusometry has been used to determine the surface to volume ratio, pore size, and tortuosity of porous materials (Callaghan, 1991; Kimmich, 1997; Stallmach and Kärger, 1999). The method has been applied to starch (Callaghan et al., 1979; Hills et al., 1998) and cellulose (Li et al., 1992, 1997) systems at varying degrees of water saturation but not previously on water-saturated samples where the bulk water is immobilized by freezing. This approach has been used on aqueous protein systems (Kimmich et al., 1990, 1993) and mesoporous silica materials (Stallmach et al., 2000). Partial freezing of the pore liquid gives rise to an increasing tortuosity of the pore space formed by the remaining liquid water. Previously it has been shown through the presence of a narrow, liquid-like resonance line at low temperatures that nonfreezing water retains local mobility. Here we show that nonfreezing water in starch granules and cellulose fibers is free to move, not only in the local environment, but also over macroscopic distances in the porous structure.

Traditional methods for characterization of porous materials, e.g., N_2-adsorption and Hg-intrusion, are necessarily performed in the dry state. Hence, they are not easily applied to biological porous materials because in these water is an essential part of the porous structure. Swelling of carbohydrate and protein gels upon addition of water is a commonly recognized phenomenon. NMR is often quoted as a noninvasive technique. The present experimental protocol with ice crystallization within the pore structure is not strictly noninvasive, but the deformation of the porous structure during freezing is less severe than the effects due to partial drying or the use of other probe liquids.

The samples studied here, pulped wood cellulose fibers and potato starch granules, can be considered as homopolymers of glucose. Because the basic chemistry is the same, the difference in water diffusion is a consequence of the supermolecular organization.

For a current review on the structure of cellulose see O'Sullivan (1997). In cellulose, the glucose units are bonded together in a β-conformation favoring straight polymer chains. Cellulose crystals are formed by the ordered

Submitted April 25, 2002, and accepted for publication July 10, 2002.

Address reprint requests to Daniel Topgaard, Lund University, P.O. Box 124, S-221 00 Lund, Sweden. Tel.: 46-46-222-01-34; Fax: 46-46-222-44-13; E-mail: daniel.topgaard@fkem1.lu.se.

0006-3495/02/12/3596/11 $2.00

FIGURE 1 Schematic section of microfibrils with 10-nm diameter in the cellulose fiber wall. The microfibrils are oriented in the direction of the fiber axis. Water diffusion is facilitated by the channels extending along the microfibrils.

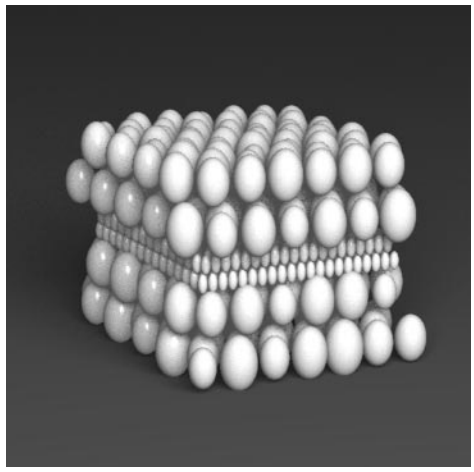

FIGURE 2 Schematic section of blocklets in a starch granule. The larger blocklets with 100-nm diameter occur in the crystalline shells, and the smaller blocklets with 30-nm diameter are situated in the semicrystalline shells. The shells are stacked in the radial direction of the granule.

packing of individual polymer chains. In wood, cellulose is in the form of rod-like microfibrils with ~10-nm width and lengths on the micrometer scale as estimated from the degree of polymerization. The microfibrils are formed during the cellulose biosynthesis. The microfibrils are in native wood encrusted by a matrix of lignin and hemicellulose. The matrix is removed during the pulping and bleaching process. The pulp fibers are in the form of flattened tubes with lengths on the millimeter scale and a wall thickness of ~10 μm. In the fiber wall, shown in Fig. 1, the microfibrils are closely packed in a parallel fashion with a preferential orientation along the fiber axis.

The present view on the structure of starch in native starch granules can be found in Gallant et al. (1997). In starch, the glucose units are bonded together in an α-conformation, which gives rise to a helical twist of the polymer chain. There are two major varieties of starch: linear amylose and branched amylopectin. Starch is in plants deposited in the form of rounded granules with a radius of tenths of micrometers. The crystalline regions are formed by the amylopectin side chains. Alternating layers of amorphous and crystalline starch form rounded blocklets with a diameter on the 50- to 500-nm scale in potato starch. Blocklets of different size form concentric shells of crystalline and semicrystalline material (compare Fig. 2). The crystal axes are oriented in the radial direction. There are amorphous channels extending in the radial direction throughout the structure.

THEORY

In this section, we present the theoretical basis for the ^{1}H NMR method to determine the amount and self-diffusion of nonfreezing water in a porous carbohydrate polymer matrix.

Nonfreezing pore liquid quantification

The macroscopic magnetization M of a sample placed in a magnetic field B_0 is related to the number of spins N and the absolute temperature T through (Abragam, 1961)

$$M = \frac{N\gamma^2\hbar^2 I(I+1)B_0}{3k_B T}, \qquad (1)$$

in which γ is the gyromagnetic ratio, $\hbar$ is the Planck constant divided by 2π, k_B is the Boltzmann constant, and I is the spin quantum number of the observed nucleus. A voltage proportional to M is induced in the receiver coil after applying a 90° radio frequency pulse. This signal, the free induction decay (FID), $S(t)$ disappears with the characteristic time constant T_2^*. Static dipolar interactions for spins residing in solid environments cause a rapid decay of the FID, and T_2^* is on the order of 10 μs. The dipolar interaction is motionally averaged in liquids, and T_2^* is between 1 ms and 1 s. From Eq. 1, it is evident that it is possible to determine the number of spins within a sample from the initial signal strength S_0. In quantitative work with T as an experimental variable, it is convenient to multiply the signal with T to arrive at a quantity that is proportional to N.

After application of a radio frequency pulse, the receiver is unable to acquire a signal from the sample for a time of ~5 to 10 μs due to interfering signals from the electronic circuits and the probe material. Signal acquisition starts after a delay denoted the receiver dead time. This time is of minor importance in the quantitative determination of liquids because of the long T_2^*. In the case of solids, it is necessary to extrapolate the signal to zero time, taken as the middle of the 90° pulse (Barnaal and Lowe, 1963), to obtain the correct value of S_0 and, thus, the number of spins. In

practice, this is achieved by fitting parts of the on-resonance time domain signal to a decaying function (Hartley et al., 1994). Depending on the lineshape, the damping of the FID has a certain functional form. For Lorentzian, Gaussian, or Voigt lineshapes, the damping is (de Beer and van Ormondt, 1992; Montigny et al., 1990; Bruce et al., 2000)

$$S(t) = S_0 \exp(-\pi w_L t) \tag{2}$$

$$S(t) = S_0 \exp\left[-\left(\frac{\pi w_G t}{2\sqrt{\ln 2}}\right)^2\right] \tag{3}$$

$$S(t) = S_0 \exp(-\pi w_L t)\exp\left[-\left(\frac{\pi w_G t}{2\sqrt{\ln 2}}\right)^2\right] \tag{4}$$

in which w_L and w_G are the Lorentzian and Gaussian half height widths of the peaks in the frequency domain. Eqs. 2 and 3 are characteristic for liquids and solids, respectively. Eq. 4 can be regarded as a Gaussian broadening of an inherently liquid-like signal.

The large difference in decay rate between signals originating from liquids and solids makes NMR a powerful tool in the study of freezing phenomena. By deliberately setting the receiver dead time to a value $3 \times T_2^*$ for the solid, it is possible to isolate the signal from the liquid. The amount of nonfreezing pore liquid as a function of T is usually determined on a relative scale. The signal arising from a solid proton-containing material can be used to make an absolute determination of the amount of nonfreezing pore liquid, expressed as mass nonfreezing liquid/mass dry solid m_{liq}/m_{sol}, if the proton density of the solid is known. Assuming that the carbohydrate material consists of condensed glucose units, the proportionality constant between m_{liq}/m_{sol} and the number of protons ratio N_{liq}/N_{sol} is 0.56. A similar value has been observed for aspen wood (Hartley et al., 1994), cellulose fibers (Topgaard and Söderman, 2001), and maize starch (Tanner et al., 1991). The use of this methodology to determine water content relies on the assumption that the liquid does not contribute to the solid-like signal and vice versa.

Transverse relaxation

Water in differing physical environments is generally characterized by different transverse relaxation time T_2. The Carr-Purcell Meiboom-Gill (CPMG) (Carr and Purcell, 1954; Meiboom and Gill, 1958) experiment, $90^\circ_x - (\tau - 180^\circ_y - \tau)_n$, is a powerful method to quantify the relative proportions of water with different values of T_2. The method has been applied to starch (Tang et al., 2000) and wood (Menon et al., 1987) systems. T_2 is shortened from the bulk value by interaction with the walls of the solid material. For a compartmentalized system, the CPMG decay curve is given by

$$S(t) = \int P(T_2) e^{-t/T_2} dT_2, \tag{5}$$

in which $P(T_2)$ is the probability density of T_2 and $t = 2n\tau$ is the time from the 90° pulse. $P(T_2)$ is deconvoluted from the experimental data through the use of a computer program such as CONTIN (Provencher, 1982). Alternatively, the parameters of a chosen distribution may be determined by assuming a functional form for $P(T_2)$. When interpreting the obtained $P(T_2)$, it is important to realize that the solution is not unique, and many different distributions satisfy the experimental data (Whittal and MacKay, 1989). In many porous systems T_2 is proportional to the pore radius. $P(T_2)$ can then be reinterpreted as a radius distribution (Whittal, 1991; Araujo et al., 1993). The main use of the CPMG experiment in this investigation is to confirm the disappearance of bulk liquid water.

Cross relaxation

Longitudinal cross relaxation between the protons of the water and the solid material is a commonly observed phenomenon in biological systems (Edzes and Samulski, 1978; Sobol et al., 1986). Transfer from water occurs via chemical exchange of protons to surface hydroxyl groups on the millisecond time scale and subsequently via dipolar interactions to the remainder of the protons in the solid on the 10- to 100-ms time scale (Oleskevich et al., 1996). The separation of time scales makes a simple two-site model an adequate description of the evolution of an actually multisite system (Tanner et al., 1991). The evolution of a two-site spin system with one solid and one liquid proton pool can be described with the coupled differential equations

$$\begin{aligned}\frac{dM_{sol}}{dt} &= -R_{1sol}(M_{sol} - M_{sol}^{eq}) - k_{sol}(M_{sol} - M_{sol}^{eq}) \\ &\quad + k_{liq}(M_{liq} - M_{liq}^{eq}) \\ \frac{dM_{liq}}{dt} &= -R_{1liq}(M_{liq} - M_{liq}^{eq}) - k_{liq}(M_{liq} - M_{liq}^{eq}) \\ &\quad + k_{sol}(M_{sol} - M_{sol}^{eq})\end{aligned} \tag{6}$$

in which M_{sol} and M_{liq} are the time-dependent solid and liquid longitudinal magnetizations with equilibrium values M_{sol}^{eq} and M_{liq}^{eq}, R_{1sol} and R_{1liq} are the intrinsic longitudinal relaxation rates, and k_{sol} and k_{liq} quantify the rate of exchange. The constants can be estimated by preparing the system in different initial states and follow the evolution. For a hydrated carbohydrate system, a convenient way to perform this is by means of the Goldman-Shen experiment (Goldman and Shen, 1966), $90^\circ_x - \tau_1 - 90^\circ_{-x} - \tau_2 -$

$90°_x$ − FID. The time τ_1 is adjusted to let M_{sol} disappear and retain variable amounts of M_{liq}. The evolution during τ_2 is followed by the third 90° pulse. For this experiment the evolution of M_{liq} is given by Peschier et al. (1996) and Topgaard and Söderman (2001)

$$M_{liq}(\tau_1, \tau_2) = M_{liq}^{eq}(1 + c^+(\tau_1)e^{-R^+\tau_2} + c^-(\tau_1)e^{-R^-\tau_2}) \quad (7)$$

in which

$$2R^{\pm} = k_{liq} + R_{1liq} + k_{sol} + R_{1sol} \pm \sqrt{(k_{liq} + R_{1liq} - k_{sol} - R_{1sol})^2 + 4k_{liq}k_{sol}} \quad (8)$$

and

$$c^{\pm}(\tau_1) = \pm\left\{\frac{M_{liq}(\tau_1) - M_{liq}^{eq}}{M_{liq}^{eq}} \times \frac{k_{liq} + R_{1liq} - R^{\mp}}{R^+ - R^-} + \frac{k_{liq}}{R^+ - R^-}\right\}. \quad (9)$$

$M_{liq}(\tau_1)$ is proportional to the slowly decaying part of the FID. Eq. 4 was found to describe the relevant parts of the FID well for the samples studied here. The sizes of the solid and liquid proton pools, p_{sol} and p_{liq}, can be calculated from

$$p_{sol} = \frac{k_{liq}}{k_{sol} + k_{liq}}, \quad p_{liq} = \frac{k_{sol}}{k_{sol} + k_{liq}}. \quad (10)$$

Diffusometry

NMR diffusometry (Callaghan, 1991; Kimmich, 1997) relies on the application of pulsed field gradients (PFGs) to determine molecular displacements on the millisecond time scale and micrometer length scale. The most common versions of the experiment use two rectangular PFGs with strength G and duration δ directed along the z-axis of the magnet. When molecular motion during the PFG can be neglected, the experiment is conveniently analyzed with a propagator formalism (Callaghan, 1991). The effect of the first PFG is to give a phase shift $-\gamma G\delta z_1$, with respect to the rotating frame of reference, to a spin at position z_1. The second PFG, applied a time t after the first one, induces a further phase shift $\gamma G\delta z_2$, in which z_2 is the new position of the spin. The total phase shift is $\gamma G\delta(z_2 - z_1)$, which equals zero for stationary spins. The phase shift depends on the dynamic displacement $Z = z_2 - z_1$ and is, thus, independent of starting position and motion transverse to the z-axis. The signal originating from one spin is proportional to $e^{i\gamma G\delta Z}$ and the total signal from the whole sample, normalized to zero gradient strength, is

$$E = \int P(Z, t)e^{i\gamma G\delta Z}dZ, \quad (11)$$

in which $P(Z, t)dZ$ is the probability that a spin moves the distance Z during the time t. For unrestricted diffusion, $P(Z, t)$ is a Gaussian function

$$P(Z, t) = \frac{1}{2\sqrt{\pi Dt}}\exp\left(-\frac{Z^2}{4Dt}\right) \quad (12)$$

with the second moment

$$\langle Z^2\rangle = 2Dt, \quad (13)$$

in which D is the self-diffusion coefficient. Inserting Eq. 12 into Eq. 11 yields

$$E = e^{-(\gamma G\delta)^2 tD}. \quad (14)$$

A more accurate analysis, taking finite PFG widths into account, gives the Stejskal-Tanner equation (Stejskal and Tanner, 1965)

$$E = e^{-kD}, \quad (15)$$

in which $k = (\gamma G\delta)^2(\Delta - \delta/3)$ and Δ is the separation between the leading edges of the PFGs. The effective diffusion time t is given by

$$t = \Delta - \delta/3. \quad (16)$$

A series expansion of the exponential in Eq. 11 yields

$$E = 1 + i\gamma G\delta\langle Z\rangle - (\gamma G\delta)^2\langle Z^2\rangle/2 + \cdots \quad (17)$$

In cases with no net flow $\langle Z\rangle = 0$ and Eq. 17 can be recast into

$$E = e^{-(\gamma G\delta)\langle Z^2\rangle/2}. \quad (18)$$

The mean square displacement can, thus, be determined from the initial slope of a plot of ln E vs. $(\gamma G\delta)^2$, irrespective of whether the diffusion is Gaussian or not. In analogy with Eq. 13, an apparent diffusion coefficient is defined through

$$D_{app} = \langle Z^2\rangle/2t \quad (19)$$

An indication of restricted diffusion within a pore with linear dimension on the order of $\langle Z^2\rangle^{1/2}$ is that D_{app} decreases with t.

NMR diffusometry in porous materials is usually performed with the stimulated echo (STE) pulse sequence, 90° − τ_1 − 90° − τ_2 − 90° − τ_1 − echo, with one PFG in each τ_1 period (Tanner, 1970). During the τ_2 period, the magnetization is stored in the longitudinal direction and is consequently protected from T_2 relaxation, which might be severe for the type of materials under investigation here. In materials containing protons, there is a risk for cross relaxation between the water and the solid, and this might influence the outcome of the experiment. More specifically, when cross relaxation occurs on the same time scale as the diffusion time, an exaggerated diffusion time dependence of the measured D may be the result if the analysis of the experiment

is based on Eq. 15. This fact could erroneously be interpreted as restricted diffusion within pores on the 10-μm scale (Li et al., 1997) or exchange between domains with different D on the 100-ms time scale (Harding et al., 2001). The analog to Eq. 15, when cross relaxation is taken into account, is (Peschier et al., 1996; Topgaard and Söderman, 2001)

$$E = e^{-kD} f(k, D, \tau_2, C, k_{liq}k_{sol}), \tag{20}$$

in which

$$f(k, D, \tau_2, C, k_{liq}k_{sol}) = e^{A\tau_2/2} \frac{\cosh(B\tau_2/2) - \frac{A + C}{B}\sinh(B\tau_2/2)}{\cosh(B_0\tau_2/2) - \frac{C}{B_0}\sinh(B_0\tau_2/2)} \tag{21}$$

and

$$\begin{aligned} A &= kD/(\Delta - \delta/3) \\ B &= \sqrt{(A + C)^2 + 4k_{liq}k_{sol}} \\ B_0 &= \sqrt{C^2 + 4k_{liq}k_{sol}} \\ C &= k_{liq} + R_{1liq} - k_{sol} - R_{1sol}. \end{aligned} \tag{22}$$

The parameters C and $k_{liq}k_{sol}$, quantifying the rate of cross relaxation, can be determined with the Goldman-Shen experiment.

Biological materials often have an anisotropic organization of their structural elements, typical examples being the organization of cellulose fibers along the trunk of a tree or nerve cell bundles along the spinal cord. Anisotropic structures may lead to anisotropic water diffusion. When working with samples consisting of randomly oriented anisotropic objects, each giving rise to a certain apparent diffusion coefficient, the total signal can be represented as an integral of the signals from the individual domains (Topgaard and Söderman, 2002a)

$$E(k) = \int P(D)E(k, D)dD, \tag{23}$$

in which $E(k, D)$ is given by Eq. 15 or Eq. 20 if cross relaxation is considered. $P(D)$ is the probability density of apparent D due to orientation effects. The use of Eq. 23 relies on the assumption that the rate of transverse-, longitudinal-, and cross-relaxation has no angular dependence. A problem is that $P(D)$ is not uniquely defined by the experimental data. The first moment of the distribution $\langle D\rangle$ is obtained by determining the initial slope of ln E vs. k. In practice, this can be done by assuming a functional form for the distribution that is consistent with the data and use $\langle D\rangle$ and the width of the distribution as adjustable parameters. One commonly used distribution is

$$P(D) = \frac{1}{D\sigma\sqrt{2\pi}} \exp\left[-\frac{1}{2}\left(\frac{\ln D - \ln\langle D\rangle - \sigma^2/2}{\sigma}\right)^2\right], \tag{24}$$

in which σ is a measure of the width of the distribution. The method based on assuming a distribution is numerically more stable than a single component fit to the initial slope, because larger parts of the data can be used in the analysis.

MATERIALS AND METHODS

Paper sheets made by bleached kraft pulp fibers were kindly supplied by SCA Research (Sundsvall, Sweden). Potato starch was obtained from Lyckeby Stärkelsen (Kristianstad, Sweden). The samples were put in 5-mm outer diameter NMR tubes and soaked with Millipore water for several days. The wet samples were kept at 5°C until experiments were performed.

NMR experiments were performed with a Bruker DMX 200 spectrometer operating at a ^{1}H frequency of 200.13 MHz. PFGs were generated in a Bruker gradient probe with a maximum gradient strength of 9.6 T/m. FIDs for the determination of amount of liquid were recorded with a dwell time of 0.5 μs after a 90° pulse with 3.6-μs duration. The receiver dead time was set to 4.5 μs. CPMG echo decay envelopes were recorded at the midpoint of even echoes with τ = 0.1 ms. The Goldman-Shen experiment was performed with 5 τ_1 values from 0.1 to 0.5 ms and 20 τ_2 values from 2 to 2000 ms. Parameters for the PFG STE experiment were: δ = 0.4 ms, three values of ($\Delta - \delta/3$) from 20 to 100 ms, and 10 equal increments of G up to 9.6 T/m for the shortest value of ($\Delta - \delta/3$). G was decreased at longer ($\Delta - \delta/3$) values to keep the k values independent of diffusion time. A 2-s delay between successive scans was sufficient for the liquid water and solid carbohydrate magnetizations to return to equilibrium.

The temperature, from −24°C to 2°C, was controlled with an accuracy of 0.2°C. NMR experiments started with temperatures above 0°C. To avoid kinetic effects at the bulk phase transition, the samples were frozen at −24°C. Experiments were then performed while approaching 0°C from subzero temperatures. The bulk ice was melted after a temperature jump to 10°C. The whole temperature cycle was repeated twice to check the reproducibility. With the procedure described above, where the bulk phase transitions took place after a temperature jump, it was found that a waiting time of 3 min was sufficient to reach equilibrium after a temperature change.

RESULTS AND DISCUSSION

Amount of nonfreezing liquid

An experimental FID obtained on a hydrated cellulose sample at a temperature of −4.6°C is shown in Fig. 3. Protons in the solid material give rise to the fast decaying component and protons in liquid domains to the component with a longer decay time. As the temperature is below the bulk freezing temperature T_m, the liquid-like signal originates from nonfreezing water. The solid-like signal is mostly due to the carbohydrate material. In principle, ice could contribute to the FID. The exceedingly long T_1 for ice prohibits the practical implementation of this method to quantify the amount of ice using the FID. In quantitative determinations of remaining liquid during freezing, the amount of solid is

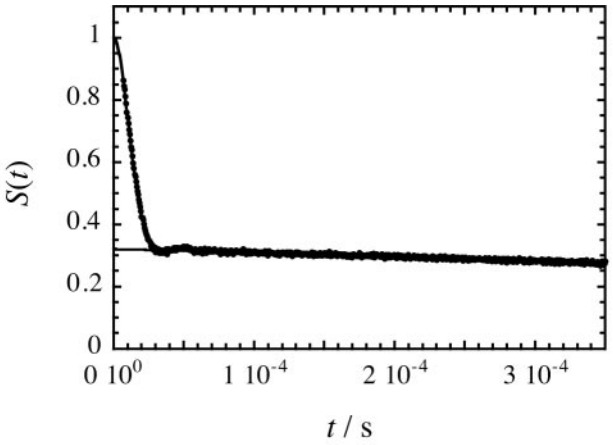

FIGURE 3 Experimental free induction decay obtained on a wet wood pulp fiber sample at −4.6°C. Points, experimental; lines, fitted. The line intersecting the *y*-axis at 0.32 represents the extrapolation of the water signal to zero time. This value is used for the quantification of the amount of nonfreezing water.

determined at a temperature above T_m where there is no interference from ice. This value, corrected for temperature effects as described previously, is then compared with the liquid signal at any temperature. The strength of the solid-like signal increases at freezing, but not in proportion to the amount of liquid that has frozen. The reason is saturation of the ice signal because of too-rapid pulsing in comparison with T_1 for ice.

The amount of nonfreezing water as a function of temperature is presented in Fig. 4. The amount of liquid water changes abruptly at 0°C because of the freezing of bulk water. The amount continues to decrease a few degrees below T_m. We attribute this to freezing of water that is confined within the porous structure but with a depressed

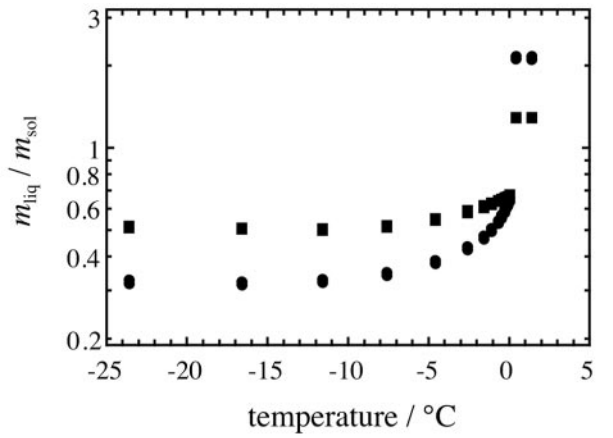

FIGURE 4 Amount of nonfreezing water as a function of temperature for wood pulp fibers (*circles*) and potato starch granules (*squares*). Experiments at each sample and temperature were repeated twice to check the reproducibility and hysteresis effects.

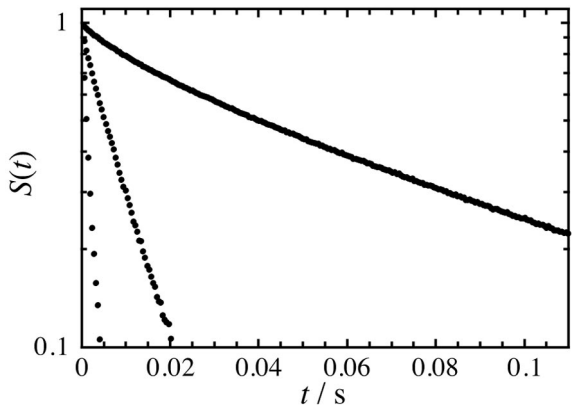

FIGURE 5 CPMG decay curves obtained on a wood pulp fiber sample at +2, −0.2, and −24°C from top to bottom. The disappearance of a component with long T_2 when changing the temperature from +2 to −0.2°C confirms the freezing of bulk water.

freezing point on account of interaction with the pore walls (Maloney and Paulapuro, 1998). Below approximately −5°C the amount is constant.

Transverse relaxation

Bulk water has much slower transverse relaxation than water confined within the porous structure. This is illustrated in Fig. 5 where selected CPMG decay curves are shown. Decreasing the temperature from slightly above to slightly below T_m leads to the disappearance of a component with T_2 on the order of 50 ms. The obvious interpretation is the freezing of bulk water. For both samples, there is a similar change at T_m. Deconvolution of CPMG decay curves is by no means straightforward, and one must realize that the result is very sensitive to the chosen method (Whittal and MacKay, 1989). The disappearance of the component with long T_2 is confirmed with both the CONTIN method and by fitting the decay curve to a sum of a small number of discrete exponentials. The signal remaining at subzero temperatures originates from nonfreezing water.

Cross relaxation

The rate of cross relaxation was quantified with the Goldman-Shen experiment. A typical outcome is shown in Fig. 6. The solid lines are Eq. 7 globally fitted to the experimental data with M_{liq}^{eq}, R_{1sol}, R_{1liq}, k_{sol}, and k_{liq} as adjustable parameters. It is evident that a two-site exchange model with one liquid and one solid component is sufficient to describe the experimental data.

Magnetization transfer from water to ice on the time scale of 1 s has been observed for a partially frozen water-polyethylene glycol system (Weglarz and Peemoeller, 1997). Ice formed from the freezing of bulk water is macroscopically separated from the nonfreezing water. It is,

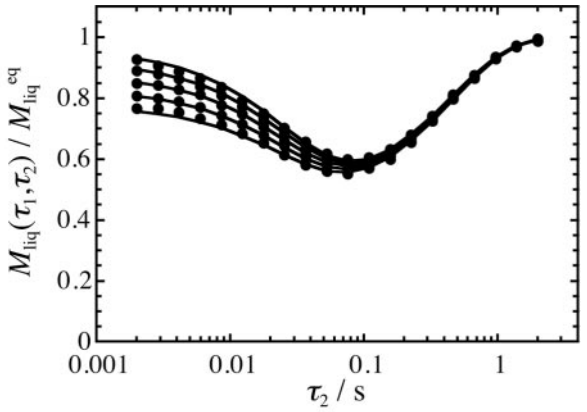

FIGURE 6 Experimental results from the Goldman-Shen cross relaxation experiment obtained on a wet wood pulp fiber sample at −4.6°C. The lines represent a global fit of Eq. 7 to the two-dimensional experimental data. τ_1 is increasing from top to bottom.

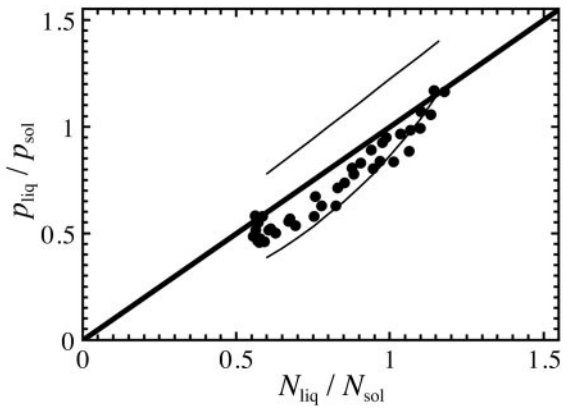

FIGURE 7 p_{liq}/p_{sol} from the cross-relaxation experiment compared with N_{liq}/N_{sol} estimated from the FID for a wet wood pulp fiber sample. The thick line indicates $p_{liq}/p_{sol} = N_{liq}/N_{sol}$. The upper thin line is calculated with the assumption that one-third of the cellulose hydroxyl protons are in chemical exchange with water on a time scale that is slower than the FID time scale but faster than the Goldman-Shen time scale. The lower thin line represents a model where ice within the fiber is a part of the solid proton pool.

therefore, unlikely that it takes part in the exchange of longitudinal magnetization. Ice within the porous structure is, however, a potential participant in the exchange. Depending on the time scale for the exchange, different effects on the outcome of the PFG STE experiment are expected. Cross relaxation occurring faster than the PFG STE time scale would have the largest impact. In this case, the measured diffusion would be a population weighted average between the contributions from the mobile nonfreezing water and the stationary ice. That this is not the case is indicated by the fact that the initial intensities of the curves with different τ_1 in Fig. 6 correspond well to the decay of the liquid-like signal in the FID. We conclude that there is no longitudinal cross relaxation between ice and water faster than 2 ms.

Another possibility is that the time for cross relaxation to ice is so close to the rate of transfer to the carbohydrate that the two processes cannot be separated. The ratio between the number of protons in the liquid and solid pools, p_{liq}/p_{sol}, can be estimated with Eq. 10. This ratio is compared with the ratio between the number of protons in the liquid and the porous matrix N_{liq}/N_{sol} in Fig. 7. If ice were a part of the solid pool, then $p_{liq}/p_{sol} < N_{liq}/N_{sol}$ would hold. From the assumption that all ice within the porous structure contribute to the solid pool, p_{liq}/p_{sol} can be estimated to $N_{liq}/(N_{sol} + N_{ice})$, in which $N_{ice} = N_{liq}^{max} - N_{liq}$.

A fraction of the protons that contribute to the solid part of the FID is in chemical exchange with the water on the millisecond time scale (Edzes and Samulski, 1978; Tanner et al., 1991), which has the result $p_{liq}/p_{sol} > N_{liq}/N_{sol}$. Previous investigations has shown that at $m_{liq}/m_{sol} = 0.2$, p_{liq}/p_{sol} is larger than N_{liq}/N_{sol} with an amount that corresponds to a fast chemical exchange with one-third of the cellulose hydroxyl groups (Topgaard and Söderman, 2001).

In conclusion, there are two processes with opposite effects: 1) chemical exchange of hydrogens between water and surface hydroxyls and 2) cross relaxation between water and ice. p_{liq}/p_{sol} calculated with the two models are compared with the experimental data in Fig. 7. The experimental results follow the trend of model 2 but is slightly higher, indicating that both processes have to be taken into account. Due to the large number of unknown variables and the scatter in the data, it is not meaningful to modify the models to obtain a better fit. What matters for the evaluation of the diffusion data is how the liquid water longitudinal magnetization evolves with time. In this context, it is of little importance if the ice contributes to the solid pool on a time scale longer than 2 ms. Faster exchange would result in measured diffusion coefficients, which are averages of the contributions from liquid water and the ice. The analysis presented above shows that this is not the case, and we can safely analyze the diffusion data with the assumption of a two site exchange, although the exact meaning of the two proton pools is uncertain.

Water self-diffusion

Nonfreezing water self-diffusion was measured with the PFG STE technique. Typical experimental results are shown in Fig. 8. Noncoincidence of the curves is generally interpreted as restricted diffusion, i.e., the diffusing molecules experience boundaries on the micrometer scale. Because cross relaxation has been shown to occur in this system, the evaluation of the experiment should be based on Eq. 20 and not Eq. 15. Moreover, we assume that a distribution of diffusion coefficients due to orientation effects can be handled with Eq. 24 (Topgaard and Söderman, 2002a). Eq. 23 with Eqs. 24 and 20 were fitted to the experimental data using $\langle D \rangle$, σ, and the initial intensity for

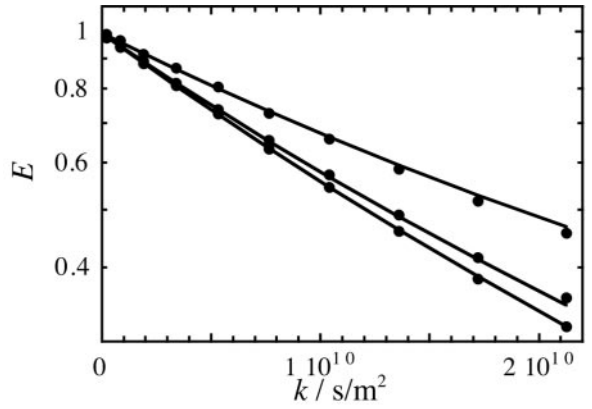

FIGURE 8 Experimental echo attenuation curves from the PFG STE experiment obtained on a wet wood pulp fiber sample at −4.6°C. The diffusion times are 20, 44.7, and 100 ms from bottom to top. The solid lines are the results of a global fit of Eq. 23 with Eqs. 20 and 24 to the experimental data using $\langle D \rangle$, σ, and the initial intensity for each curve as adjustable parameters.

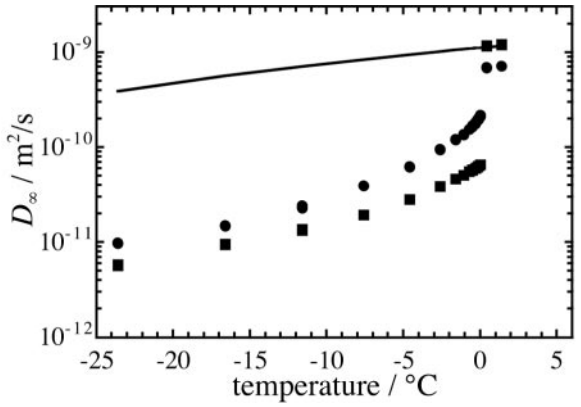

FIGURE 9 D_∞ of nonfreezing water as a function of temperature for wood pulp fibers (*circles*) and potato starch granules (*squares*). The line represents the diffusion coefficient of supercooled water (Price et al., 1999), D_0.

each curve as adjustable parameters. The parameters C and $k_{liq}k_{sol}$ quantifying the cross relaxation were determined with the Goldman-Shen experiment as described above. In most cases, $\langle D \rangle$ was independent of the value of the diffusion time, implying that restricted diffusion is not at hand. The curves do not coincide because of the presence of cross relaxation. To improve the accuracy of the estimated value of $\langle D \rangle$, we performed a global fit to the experimental data with the condition that $\langle D \rangle$ and σ should be independent of diffusion time. A notable exception to the independence of $\langle D \rangle$ on t was observed for the cellulose sample at the temperatures just below T_m. Here $\langle D \rangle$ decreased ~20% with increasing t. This behavior has previously been interpreted as the existence of pores with one dimension on the micrometer scale (Topgaard and Söderman, 2002b). In this contribution, we do not pursue this issue further and instead focus on the interpretation of $\langle D \rangle$ obtained at long t. This value, D_∞, is a measure of the long-range connectivity of the porous network.

D_∞ for water sorbed in carbohydrate materials as a function of temperature is shown in Fig. 9. At temperatures above T_m water both inside and outside the porous objects contribute to the measured diffusion and cross relaxation. No attempts were made to separate the contributions. The values above T_m are displayed to show that the presence of bulk water leads to a much faster diffusion than what can be observed below T_m. The values are monotonously increasing with temperature. At the same temperature as the ice within the porous matrix starts to melt, there is an upturn of D_∞. Nonfreezing water in mesoporous silica materials has been shown to have the same temperature dependence as free supercooled water (Stallmach et al., 2000). Therefore, it is reasonable to normalize D_∞ with the temperature-dependent bulk value D_0 (Price et al., 1999) to acquire a quantity that is a temperature-independent measure of the connectivity of the porous network. A comparison of Figs. 4 and 9 shows that the amount of liquid water has a large impact on the connectivity. The ice within the porous material acts by blocking diffusion paths for the remaining liquid water. It is not likely that any pores are completely frozen out, because in the contact area between ice and a hydrophilic solid surface there is always a liquid film with a thickness of one or a few nanometers depending on the temperature (Churaev et al., 2002; Kuz, 1997). Freezing of a pore with transverse dimension on the order of 10 nm would not completely block the transport through the pore as long as the liquid film remains. At the lowest temperatures all diffusion occurs in channels with a thinnest dimension of a few diameters of a water molecule. A pictorial representation of the pore space during freezing is shown in Fig. 10.

The tortuosity factor α is a function of both the volume fraction of the pore liquid and how curved and tortuous the diffusion paths are. α is defined from self-diffusion measurements as (Bear, 1988; Latour et al., 1995; Stallmach and Kärger, 1999)

$$\frac{1}{\alpha} = \frac{D_\infty}{D_0}. \tag{25}$$

α is a purely geometrical property of pore space, and the definition in Eq. 25 is meaningful only when the pore liquid locally diffuses with D_0. The interaction between the pore walls and the liquid has to be considered when dealing with systems where the pore liquid consists of only a few molecular layers. $1/\alpha$ calculated with Eq. 25 versus amount of nonfreezing water is plotted in Fig. 11. The analysis ignores the effect of fast chemical exchange of hydrogen between water and carbohydrate hydroxyl groups situated at surfaces of the pore walls and the reduced mobility of the water that interacts most strongly with the solid material. The effect of chemical exchange could in principle be quantified from

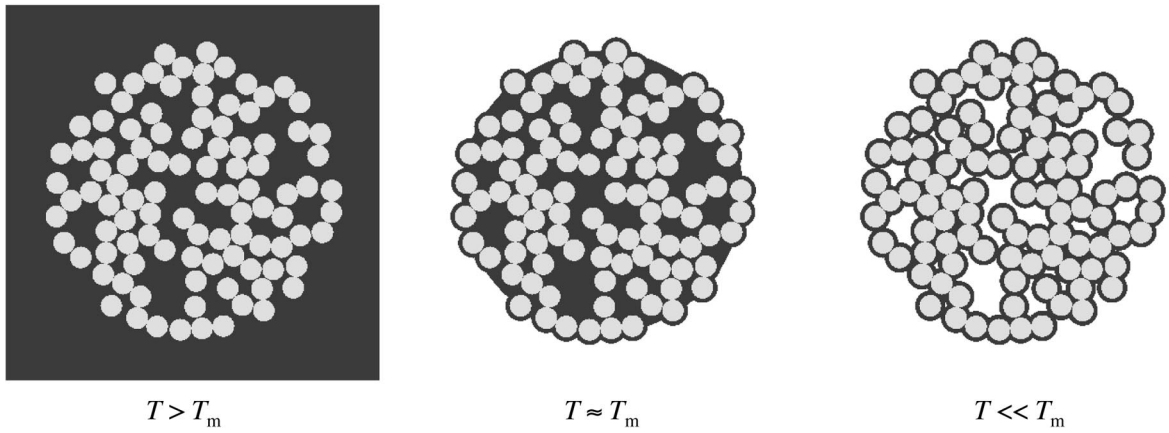

FIGURE 10 Schematic picture of the pore space of a porous carbohydrate material during gradual freezing. The circles represent solid carbohydrate material. The proportions between solid and liquid are representative for cellulose fibers swollen in water. The circles can be interpreted as cross sections of rod-like cellulose microfibrils with a diameter of 10 nm. Water and ice is depicted as gray and white, respectively. Decreasing T to slightly below T_m leads to freezing of the water outside the porous material. At this stage the measured D_∞/D_0 of water is a measure of the tortuosity of the water-saturated porous material. Further decrease of T induces ice formation within the porous structure.

Fig. 7. As discussed above, there are too many unknown parameters for this to be accomplished. We estimate that the reduction in diffusion due to chemical exchange between water and surface hydroxyls is around 10%.

Interpretation in terms of structure

The majority of the knowledge about cellulose and starch ultrastructure is based on electron microscopy. This technique says little about the position of water within the structures. Water is excluded from the crystalline regions with the exception of a small amount that is situated within the crystalline amylopectin helix in potato starch. The presence of different types of water is supported by the fact that some water freezes at a temperature below T_m, and some water does not appear to freeze at all. We will denote the two fractions as freezable and unfreezable, respectively. The two fractions constitute the nonfreezing water with thermodynamic properties different from bulk water. Because there is always a liquid film with thickness of order 1 nm surrounding the ice, freezable water must be situated in spaces with a smallest linear dimension on the 10-nm scale. A reasonable location for such voids is between microfibrils and blocklets in cellulose and starch, respectively.

The cellulose area accessible for water sorption has been estimated to $\sim$200 m^2/g (Topgaard and Söderman, 2001). This value is consistent with water sorption taking place at the surface of 10-nm diameter microfibrils. The amount of unfreezable water, 0.3 g of water per gram of carbohydrate, corresponds to a layer with $\sim$1-nm thickness surrounding the microfibrils. Based on these facts, we interpret unfreezable water as a 1-nm layer surrounding the microfibrils and freezable water as filling the space between microfibrils.

The corresponding assignment is more complicated for starch due to the structural complexity. Water will in this case be situated within the crystalline amylopectin helix, in the amorphous lamellae of the blocklets, in the radial amorphous channels, and at the blocklet surfaces. This explains the comparatively higher amount of unfreezable water, 0.5 g of water per gram of carbohydrate. The requirement for a certain size of the pores for the water to be able to freeze makes the spaces between the blocklets the only reasonable location for freezable water.

The differences in water diffusion can also be explained through the assignments made above. In a pulp fiber the water is situated in the space between rod-like microfibrils, which extend a few micrometers along the axis of the fiber. The water diffusion is facilitated by the extended channels along the microfibrils. The channels do not necessarily extend uninterrupted along the full length of the microfibrils because of the irregular and twisting pattern in which the microfibrils are packed (see Fig. 1). Partial freezing of the water within the porous structure blocks the largest channels that are the most effective for water diffusion. Decreasing temperature leads to a gradual freezing of smaller pores and a decreasing thickness of the liquid film surrounding the previously frozen pores, both factors hindering the motion of the remaining liquid water.

The slowest diffusion is exhibited by the potato starch sample. The small amount of freezable water shows that the larger mode pores that facilitate diffusion in wood pulp fibers are less important in starch granules. The slower diffusion in starch is also due to the pore geometry. Although the smallest dimension of the pores in cellulose and starch are of the same size, the longest dimension is an order of magnitude larger in cellulose.

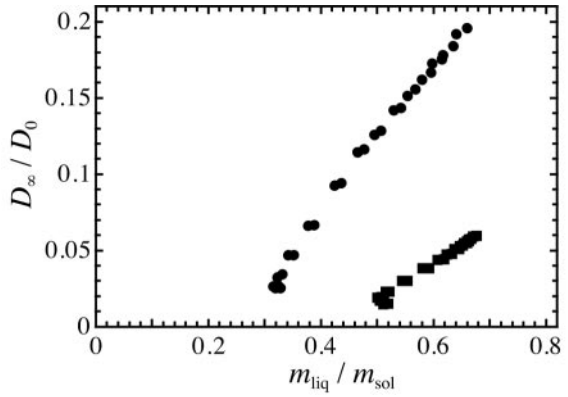

FIGURE 11 D_∞/D_0 as a function of amount of nonfreezing water for wood pulp fibers (*circles*) and potato starch granules (*squares*). If the nonfreezing water diffuses locally with D_0, then D_∞/D_0 equals the inverse tortuosity $1/\alpha$, which is a purely geometric property of the pore space.

An indication that the local self-diffusion of the freezable water is not very different from bulk water is constituted by the fact that the data for the lowest temperatures collapse into a single point in Fig. 11 when normalized with the temperature dependent D_0. This shows that the diffusion of the supercooled bulk water and the unfreezable water have the same temperature dependence and thus activation energy for diffusion in the temperature range -5°C to -25°C.

It is not *a priori* evident that the liquid water remaining at the lowest temperatures should be free to move throughout the structure, compare with Kimmich et al. (1990) where nonfreezing water was found to be trapped around isolated protein molecules at protein concentrations below the percolation threshold. The results indicate that the ice within the porous structure does not encapsulate the structural elements, keeping the still liquid water trapped. Instead, the water is free to move throughout the porous structure, presumably via regions where the structural objects are in close contact. This is illustrated by the fact that at -24°C, the water in the pulp fiber sample has a root mean square displacement of 1.4 μm during 0.1 s.

CONCLUSIONS

NMR diffusometry is used to follow water diffusion in water-swollen porous carbohydrate polymer systems at subzero temperatures. The amount of liquid water as a function of temperature is determined on an absolute scale from the free induction decay. The analysis of the diffusometry experiments takes cross relaxation between liquid water and protons in a solid environment (carbohydrate and ice) into account. Apart from bulk water, two water fractions with different freezing behavior is detected: freezable water with a freezing temperature between approximately -5°C and 0°C and water, which remains liquid even at -24°C. The latter class of water is interpreted as a water layer with approximate thickness 1 nm surrounding and, for starch, penetrating into the carbohydrate structural elements. Freezable water is situated in voids with a smallest dimension on the 10-nm length scale. The tortuosity of the porous network is rationalized in terms of the ultrastructure known from electron microscopy. The slower diffusion of water in starch granules in comparison to cellulose fibers is attributed to the smaller amount of freezable water and the pore geometry. Nonfreezing water is free to move throughout the porous structure even at temperatures where a substantial amount of the water inside the porous structure is frozen. We believe that the method presented here has general applicability to biological systems consisting of water and solid carbohydrate, protein, or lipid.

This work was financially supported by the Colloid and Interface Technology program of the Swedish Foundation for Strategic Research.

REFERENCES

Abragam, A. 1961. The Principles of Nuclear Magnetism. Oxford University Press, London.

Araujo, C. D., A. L. MacKay, K. P. Whittal, and J. R. T. Hailey. 1993. A diffusion model for spin-spin relaxation of compartmentalized water on wood. *J. Magn. Reson. B.* 101:248–261.

Barnaal, D., and I. J. Lowe. 1963. Effects of rotating magnetic fields on free-induction decay shapes. *Phys. Rev. Lett.* 11:258–260.

Bear, J. 1988. Dynamics of Fluids in Porous Media. Dover Publications, New York.

Bruce, S. D., J. Higinbotham, I. Marshall, and P. H. Beswick. 2000. An analytical derivation of a popular approximation of the Voigt function for the quantification of NMR spectra. *J. Magn. Reson.* 142:57–63.

Callaghan, P. T. 1991. Principles of nuclear magnetic resonance microscopy. Oxford University Press, Oxford.

Callaghan, P. T., K. W. Jolley, and J. Lelievre. 1979. Diffusion of water in the endosperm tissue of wheat grains as studied by pulsed field gradient nuclear magnetic resonance. *Biophys. J.* 28:133–141.

Carr, H. Y., and E. M. Purcell. 1954. Effects of diffusion on free precession in nuclear magnetic resonance experiments. *Phys. Rev.* 94:630–638.

Churaev, N. V., V. D. Sobolev, and V. M. Starov. 2002. Disjoining pressure of thin nonfreezing interlayers. *J. Colloid Interface Sci.* 247: 80–83.

de Beer, R., and D. van Ormondt. 1992. Analysis of NMR data using time domain fitting procedures. *NMR Basic Princ. Progr.* 26:201–248.

Edzes, H. T., and E. T. Samulski. 1978. The measurement of cross-relaxation effects in the proton NMR spin-lattice relaxation of water in biological systems: hydrated collagen and muscle. *J. Magn. Reson.* 31:207–229.

Furó, I., and J. Daicic. 1999. NMR cryoporometry: a novel method for the investigation of the pore structure of paper and paper coatings. *Nordic Pulp Paper Res. J.* 14:221–225.

Gallant, D. J., B. Bouchet, and P. M. Baldwin. 1997. Microscopy of starch: evidence of a new level of granule organization. *Carbohydr. Polymers.* 32:177–191.

Goldman, M., and L. Shen. 1966. Spin-spin relaxation in LaF_3. *Phys. Rev.* 144:321–331.

Hansen, E. W., M. Stöcker, and R. Schmidt. 1996. Low-temperature phase transition of water confined in mesopores probed by NMR: influence on pore size distribution. *J. Phys. Chem.* 100:2195–2200.

Hansen, E. W., E. Tangstad, E. Myrvold, and T. Myrstad. 1997. Pore structure of mesoporous/microporous materials by ^{1}H NMR using water as a probe molecule. *J. Phys. Chem. B.* 101:10709–10714.

Harding, S. G., D. Wessman, S. Stenström, and L. Kenne. 2001. Water transport during the drying of cardboard studied by NMR imaging and diffusion techniques. *Chem. Eng. Sci.* 56:5269–5281.

Hartley, I. D., F. A. Kamke, and H. Peemoeller. 1994. Absolute moisture content determination of aspen wood below the fiber saturation point. *Holzforschung.* 48:474–479.

Hills, B. P., J. Godward, C. E. Manning, J. L. Biechlin, and K. M. Wright. 1998. Microstructural characterization of starch systems by NMR relaxation and q-space microscopy. *Magn. Reson. Imaging.* 16:557–564.

Ishikiriyama, K., and M. Todoki. 1995. Pore size distribution measurements of silica gels by means of differential scanning calorimetry. II. Thermoporosimetry. *J. Colloid Interface Sci.* 171:103–111.

Jackson, C. L., and G. B. McKenna. 1990. The melting behavior of organic materials confined in porous solids. *J. Chem. Phys.* 93:9002–9011.

Kimmich, R. 1997. NMR: Tomography, Diffusometry, Relaxometry. Springer-Verlag, Berlin.

Kimmich, R., T. Gneiting, K. Kotitschke, and G. Schnur. 1990. Fluctuations, exchange processes, and water diffusion in aqueous protein systems: a study of bovine serum albumin by diverse NMR techniques. *Biophys. J.* 58:1183–1197.

Kimmich, R., F. Klammler, V. D. Skirda, I. A. Serebrennikova, A. I. Maklakov, and N. Fatkullin. 1993. Geometrical restrictions of water diffusion in aqueous protein systems: a study using NMR field-gradient techniques. *Appl. Magn. Reson.* 4:425–440.

Kuz, V. A. 1997. Thermal behavior of a nonfreezing water interlayer. *J. Colloid Interface Sci.* 190:114–117.

Latour, L. L., R. L. Kleinberg, P. P. Mitra, and C. H. Sotak. 1995. Pore-size distributions and tortuosity in heterogeneous porous media. *J. Magn. Reson. A.* 112:83–91.

Li, S., L. C. Dickinson, and P. Chinachoti. 1998. Mobility of "unfreezable" and "freezable" water in waxy corn starch by ^{2}H and ^{1}H NMR. *J. Agric. Food Chem.* 46:62–71.

Li, T.-Q., U. Henriksson, T. Klason, and L. Ödberg. 1992. Water diffusion in wood pulp cellulose fibers studied by means of the pulsed gradient spin-echo method. *J. Colloid Interface Sci.* 154:305–315.

Li, T.-Q., M. Häggkvist, and L. Ödberg. 1997. Porous structure of cellulose fibers studied by q-space NMR imaging. *Langmuir.* 13:3570–3574.

Maloney, T. C., and H. Paulapuro. 1998. Hydration and swelling of pulp fibers measured with differential scanning calorimetry. *Nordic Pulp Paper Res. J.* 1:31–36.

Meiboom, S., and D. Gill. 1958. Modified spin-echo method for measuring nuclear relaxation times. *Rev. Sci. Instruments.* 29:688–691.

Menon, R. S., A. L. MacKay, J. R. T. Hailey, M. Bloom, A. E. Burgess, and J. S. Swanson. 1987. An NMR determination of the physiological water distribution in wood during drying. *J. Appl. Polymer Sci.* 33: 1141–1155.

Montigny, F., J. Brondeau, and D. Canet. 1990. Analysis of time-domain NMR data by standard non-linear least squares. *Chem. Phys. Lett.* 170:175–180.

O'Sullivan, A. 1997. Cellulose: the structure slowly unravels. *Cellulose.* 4:173–207.

Oleskevich, D. A., N. Gharamany, W. P. Weglarz, and H. Peemoeller. 1996. Interfacial spin-spin coupling in wood by 2D time-domain NMR. *J. Magn. Reson. B.* 113:1–8.

Overloop, K., and L. Van Gerven. 1993. Freezing phenomena in adsorbed water as studied by NMR. *J. Magn. Reson. A.* 101:179–187.

Peschier, L. J. C., J. A. Bouwstra, J. de Bleyser, H. E. Junginger, and J. C. Leyte. 1996. Cross-relaxation effects in pulsed-field-gradient stimulated-echo measurements on water in a macromolecular matrix. *J. Magn. Reson. B.* 110:150–157.

Price, W. S., H. Ide, and Y. Arata. 1999. Self-diffusion of supercooled water to 238 K using PGSE NMR diffusion measurements. *J. Phys. Chem. A.* 1999:448–450.

Provencher, S. W. 1982. CONTIN: a general purpose constrained regularization program for inverting noisy linear algebraic and integral equations. *Computer Phys. Comm.* 27:229–242.

Sobol, W. T., I. G. Cameron, W. R. Inch, and M. M. Pintar. 1986. Modeling of proton spin relaxation in muscle tissue using nuclear magnetic resonance spin grouping and exchange analysis. *Biophys. J.* 50:181–191.

Stallmach, F., and J. Kärger. 1999. The potentials of pulsed field gradient NMR for investigation of porous media. *Adsorption.* 5:117–133.

Stallmach, F., J. Kärger, C. Krause, M. Jeschke, and U. Oberhagemann. 2000. Evidence of anisotropic self-diffusion of guest molecules in nanoporous materials of MCM-41 type. *J. Am. Chem. Soc.* 122:9237–9242.

Stejskal, E. O., and J. E. Tanner. 1965. Spin diffusion measurements: spin echoes in the presence of a time-dependent field gradient. *J. Chem. Phys.* 42:288–292.

Strange, J. H., M. Rahman, and E. G. Smith. 1993. Characterization of porous solids by NMR. *Phys. Rev. Lett.* 71:3589–3591.

Tang, H.-R., J. Godward, and B. Hills. 2000. The distribution of water in native starch granules - a multinuclear NMR study. *Carbohydr. Polymers.* 43:375–387.

Tanner, J. E. 1970. Use of stimulated echo in NMR diffusion studies. *J. Chem. Phys.* 52:2523–2526.

Tanner, S. F., B. P. Hills, and R. Parker. 1991. Interactions of sorbed water with starch studied using proton nuclear magnetic resonance spectroscopy. *J. Chem. Soc. Faraday Trans.* 87:2613–2621.

Topgaard, D., and O. Söderman. 2001. Diffusion of water absorbed in cellulose fibers studied with ^{1}H-NMR. *Langmuir.* 17:2694–2702.

Topgaard, D., and O. Söderman. 2002a. Self-diffusion in two- and three-dimensional powders of anisotropic domains: an NMR study of the diffusion of water in cellulose and starch. *J. Phys. Chem. B.* In press.

Topgaard, D., and O. Söderman. 2002b. Changes of cellulose fiber wall structure during drying investigated using NMR self-diffusion and relaxation experiments. *Cellulose.* 9:139–147.

Vittadini, E., L. C. Dickinson, and P. Chinachoti. 2001. ^{1}H and ^{2}H NMR mobility in cellulose. *Carbohydr. Polymers.* 46:49–57.

Weglarz, W. P., and H. Peemoeller. 1997. Observation of coupling across the ice-water interface by 2D time domain NMR. *J. Magn. Reson.* 124:484–485.

Whittal, K. P. 1991. Recovering compartment sizes from NMR relaxation data. *J. Magn. Reson.* 94:486–492.

Whittal, K. P., and A. L. MacKay. 1989. Quantitative interpretation of NMR relaxation data. *J. Magn. Reson.* 84:134–152.